Improvement of the total focusing method using an inverse problem approach

Ewen Carcreff, Nans Laroche and Dominique Braconnier
The Phased Array Company
9365 Allen Road
West-Chester, Ohio, USA
ewen.carcreff@thephasedarraycompany.com

Sébastien Bourguignon
Laboratoire des Sciences du Numérique de Nantes
1 rue de la Noë
44321 Nantes, France
sebastien.bourguignon@ls2n.fr

Aroune Duclos
Laboratoire d'Acoustique de l'Université du Maine
Avenue Olivier Messiaen
72085 Le Mans, France
aroune.duclos@univ-lemans.fr

***Abstract*—Imaging using the total focusing method (TFM) is a popular tool, which is becoming a standard, for nondestructive testing and evaluation. From full matrix capture data, it consists in focusing at each point of a defined reconstruction zone. It is generally more efficient than conventional phased array focusing, which only focuses at a few points. Despite its good image quality, TFM suffers from a lack of resolution and contrast, in particular in the case of close defects or in scattering materials. The TFM algorithm can be formalized as a linear operation on the data. The contribution of this paper is then to include a sparsity-inducing penalization to the TFM procedure. The reconstructed image is therefore supposed to contain only a few non zero values, corresponding to flaws or geometry. The final image is obtained by minimizing a penalized least-squares criterion within an iterative procedure. A first example uses data acquired from two close side drilled holes (SDH) in an aluminum block. The proposed algorithm shows good echo separation whereas the reference method suffers from overlapping, demonstrating resolution improvement. A second example comes from a stainless steel specimen, with high scattering noise level. The proposed method reduces the scattering noise and improves the contrast.**

***Index Terms*—Ultrasonic imaging, nondestructive testing and evaluation, total focusing method, inverse problem, sparsity.**

I. Introduction

Ultrasonic imaging using phased-array probes is now a standard in nondestructive evaluation and medical imaging. The conventional way to perform imaging is to apply a delay law on the elements directly from the hardware in order to focus the beam at a specific point of the inspected specimen. This operation is repeated several times to focus at several points. This method hence consists in applying beamforming both in transmission and reception. Another family of methods consists in transmitting an unfocused beam and to perform focusing only in reception by post-processing the data. In this family, we can cite the synthetic aperture focusing technique (SAFT) [1] and the total focusing method (TFM) [2], [3]. In SAFT, the data are composed of all independent signals of the array whereas in TFM, the data contain all inter-element impulse responses of the array. TFM generally gives better performances than conventional imaging in terms of resolution and contrast. All such techniques can be considered as *generic* and somehow naive because they do not consider any *a priori* information about the structure of the object to reconstruct. This leads to a limited resolution and a limited contrast. Our goal is to propose a method that improves resolution and contrast for TFM data, by incorporating prior assumptions on the image to be reconstructed. Improving resolution is important for separating closed reflectors. Improving contrast will enable a better detection of flaws in presence of noise, in particular in scattering materials.

An alternative to such basic approaches considers TFM reconstruction as an inverse problem, where the purpose is to reconstruct an estimation of the object under test [4]. Usually, these methods consider a point spread function (PSF) in the direct model. The PSF can be measured or parameterized by an analytic model. In [5], the Excitelet algorithm uses a PSF in a matched filter approach (cross-correlation) for TFM data. This method gives good results but does not consider any specific structure of the object, which may lead to overlapping signatures for close reflectors. Other works consider both a PSF model and some regularization of the inverse problem [6]–[8]. This regularization reinforces a specific structure of the object. Nevertheless, these papers only account for SAFT data, which is a more simple configuration than TFM.

This paper presents an inverse approach considering directly the TFM model and a sparse regularization [9]–[11], which stands for point-like reflectors. The benefit of this model is that no PSF needs to be considered, *i.e.* no deconvolution is considered. This avoids the problem of PSF estimation or cases where the waveform is varying due to attenuation [12], diffraction [13], *etc.* This point offers a greater flexibility in the imaging process.

This paper is organized as follows. The second section presents the inversion approach that we developed. Here, we also define the direct model that is employed. The third section shows some result examples from real experimental data. In

978-1-5386-3383-0/17/$31.00 ©2017 IEEE

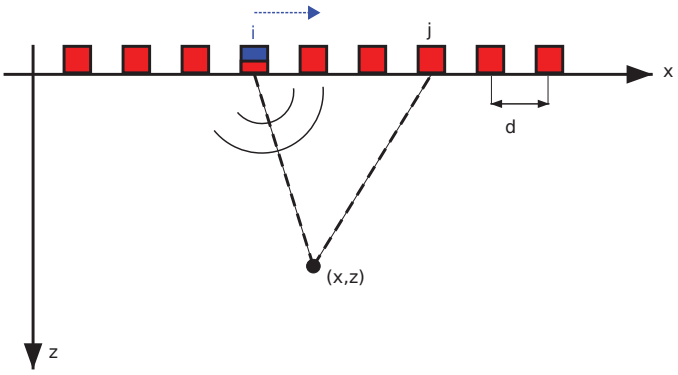

Fig. 1. Concept of TFM data acquisition. A single element is transmitting a pulse (in blue) and the signals are received by all transducers (in red). This operation is performed for all transmitting elements.

particular, we focus on examples showing close reflectors and scattering noise. The conclusion in Section IV closes the paper.

II. Inversion method

A. Total focusing method model

The acquisition process of the total focusing method (TFM) consists in recording all inter-element signals, as described in Fig. 1. The time-domain signal acquired from emitter i and receiver j is denoted $y(t,i,j)$ where i and j index the transmitting and the receiving elements, placed in $(x_i,0)$ and $(x_j,0)$, respectively (spatial coordinates refer to the (x,z) plane, see Fig. 1). If N is the total number of elements, the data set is defined by $y(t,i,j)$ for $i=1\dots N$ and $j=1\dots N$. The standard TFM reconstruction of the image at any point (x,z) is then given by [3]

$$o(x,z)=\sum_{i,j} y\left(\frac{\sqrt{(x-x_i)^2+z^2}+\sqrt{(x-x_j)^2+z^2}}{c},i,j\right). \quad (1)$$

The acoustic velocity c is supposed to be constant, underlying that the medium under test is homogeneous and isotropic. The computation formulated by (1) is equivalent to focus at each point (x,z), that is why it is called total focusing method. The output image is defined by a reconstruction grid in x and z directions.

From (1), we can deduce that TFM imaging is equivalent to a linear operator applied to data

$$\boldsymbol{o}=\mathbf{B}^T\boldsymbol{y}, \quad (2)$$

where $\boldsymbol{o}$ is a vectorized representation of the output image, $\boldsymbol{y}$ is a vectorized representation of all the data and $\mathbf{B}$ is a binary matrix containing *one* values at the proper positions. The matrix $\mathbf{B}$ depends only on the geometry of the inspection. It can be seen as a beamforming operator, linearly building the TFM image from raw data.

B. Proposed inverse method

The principle of the proposed method is to consider the underlying TFM model in a standard inverse problem approach [4]. This model is defined by $\boldsymbol{y}=\mathbf{B}\boldsymbol{o}+\boldsymbol{e}$ where the vector $\boldsymbol{e}$ accounts for noise and model errors. The aim of the inverse problem is then to minimize a criterion

$$J(\boldsymbol{o})=\|\boldsymbol{y}-\mathbf{B}\boldsymbol{o}\|^2+\mu\phi(\boldsymbol{o}), \quad (3)$$

where $\phi(\boldsymbol{o})$ is a regularization function and μ is a regularization parameter. The criterion $J(\boldsymbol{o})$ is then a trade-off between the least-squares fit and the regularization, the rate being tuned by μ. In the present paper, we have chosen a sparsity-inducing regularization using an ℓ_1-norm [10], which means that the image will have many zero values. By this choice, we assume that the object under ultrasonic inspection has a sparse reflectivity map, that is, it contains only a few reflectors. The ℓ_1-norm has become a standard choice in the literature about sparsity, which promotes sparsity while preserving the convexity of criterion (3), allowing optimization to be addressed through dedicated algorithms [14].

Due to the large dimension of the optimization problem, we used an iterative local optimization procedure. The algorithm is stopped when the norm of the difference between two iterates is inferior to a tolerance. In this paper, this inverse method is denoted TFMp for penalized TFM. Note that the proposed method can be applied to any acquisition scheme (SAFT, TFM, *etc.*).

C. Setting the regularization parameter

There are several manners to set the regularization parameter:

- The parameter can be set by the user through some trial-and-error procedure.
- It can be set at a fixed percentage of the maximal parameter value, $\mu_{max}=\left\|\mathbf{B}^T\boldsymbol{y}\right\|_\infty$. μ_{max} is the value of μ under which the reconstructed object has non-zero values. Note that in the nondestructive testing examples that we give below, μ was always set between 40% and 80% of μ_{max}.
- Automatic methods exist such as matching to noise level, cross validation [15], [16] or informational criteria [17].
- A more pragmatical choice would be to use a calibration specimen containing a target flaw to detect. The parameter μ is then set by the operator in order that the target flaw is well detected with a satisfactory contrast.

In the present study, examples consist in calibration pieces with known ground truth. Therefore, the parameter μ was tuned manually in order to obtain the best visual results with acceptable contrast.

III. Results from real data

We now present results obtained in application to experimental data. The data are acquired with an open platform, the OEM-PA manufactured by Advanced OEM Solution (AOS)[1]. This device allows open acquisition patterns, such as full parallel reception, and full access to raw data.

[1] www.aos-ndt.com

978-1-5386-3383-0/17/$31.00 ©2017 IEEE

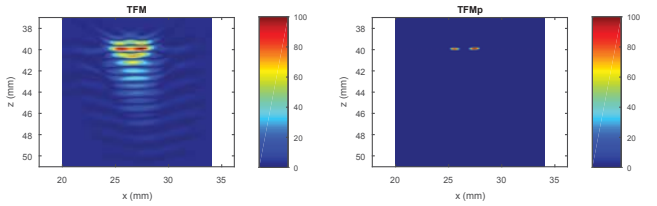

Fig. 2. Images obtained by TFM and TFMp for the first example with two close reflectors. TFMp is tuned with $\mu = 80\ \%\ \mu_{max}$.

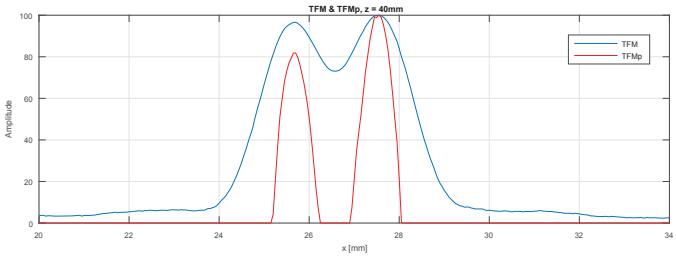

Fig. 3. Line for $z = 40$ mm for the first example with two close reflectors.

A. Metrics for evaluation

Metrics have been employed in order to quantify the resolution and contrast, that are the two main improvements targeted by our method. The resolution will be evaluated as the full width at half maximum (FWHM) of the reflector in both axial and lateral directions. This is equivalent to measure the width of the reflector at -6 dB. We also compute contrast to noise ratio (CNR) in dB that is a standard contrast metric [18]:

$$\mathrm{CNR} = 10 \log \frac{|o_{\max} - o_n|^2}{\sigma_n^2}, \tag{4}$$

where $o_{\max}$ is the maximum value of the reflector, o_n is the mean value in a noisy area and σ_n is the standard deviation in the noise. Note that the proposed algorithm can give $\mathrm{CNR} = \infty$: in noisy regions, the sparsity constraint may yield $o_n = 0$ and $\sigma_n = 0$.

B. Two close reflectors in aluminum

The first example is the inspection in contact of a thick aluminum block containing two side drilled holes (SDH). The SDH have diameter 1 mm and are spaced by 2 mm center to center, meaning that the edges are separated by 1 mm. The depth of the SDH is 40 mm. The phased array probe has 64 elements and the pitch is 0.8 mm. It center frequency is 3 MHz, meaning that the wavelength in aluminum is about 2.2 mm. The images obtained by TFM and TFMp are displayed in Fig. 2 and the line corresponding to $z = 40$ mm (where the SDH are located) as a function of x is plotted in Fig. 3. The strong overlapping is clearly visible in the TFM reconstruction due to the reflectors proximity with respect to wavelength. The metrics obtained by the two methods are given in Tab. I. With the proposed algorithm, the resolution, both in lateral and axial directions, are clearly improved. It is important to note that the lateral resolution is high for TFM because the -6 dB drop actually includes both reflectors. About contrast, the advantage of the TFMp approach is that it gives an infinite CNR compared to TFM in such cases (this was expected in homogeneous materials).

C. Five reflectors in aluminum

This example is pretty similar to the first one, with five SDH, with diameter 1 mm, spaced by 7, 5, 4, 3 mm center to center and located at depth $z = 20$ mm. The same probe is employed in contact. The reconstructed images and associated metrics are given in Fig. 4 and Tab. II, respectively. Flaws are coherently detected and scaled with TFMp, whereas TFM reconstruction shows many oscillations and artifacts. The lateral resolution improvement is between a factor of 2 and 3. The axial resolution improvement is about a factor of 8.

TABLE I
METRICS FOR THE FIRST EXAMPLE

	TFM		**TFMp**	
	Res. (mm)	***CNR (dB)***	***Res. (mm)***	***CNR (dB)***
Reflector #1	x: 3.64 z: 1.57	29.8	x: 0.70 z: 0.14	∞
Reflector #2	x: 3.60 z: 1.86	30.1	x: 0.75 z: 0.16	∞

TABLE II
METRICS FOR THE SECOND EXAMPLE

	TFM		**TFMp**	
	Res. (mm)	***CNR (dB)***	***Res. (mm)***	***CNR (dB)***
Reflector #1	x: 1.33 z: 1.47	24.7	x: 0.43 z: 0.18	∞
Reflector #2	x: 1.16 z: 1.49	25.7	x: 0.52 z: 0.21	∞
Reflector #3	x: 1.16 z: 1.46	25.4	x: 0.51 z: 0.19	∞
Reflector #4	x: 1.28 z: 1.45	24.7	x: 0.51 z: 0.17	∞
Reflector #5	x: 1.38 z: 1.45	24.5	x: 0.55 z: 0.17	∞

D. Side drilled holes in stainless steel

The third example is taken from a stainless steel block containing three diagonally-spaced SDH (∅ 1.6 mm). It is inspected using a probe in contact with 64 elements and pitch 1 mm. The center frequency is 5 MHz which gives a wavelength of about 1.9 mm in this material. This specimen has a coarse grained structure so that the ultrasonic waves suffer from scattering noise. The reconstructed images are displayed in Fig. 5. The scattering noise is highly present in the TFM image reaching about 50% of the maximum scale. The lines corresponding to the center of the second SDH are plotted in Fig. 3. The metrics are given in Tab. III. The resolution and contrast improvements are important. Note that for the third reflector, the resolution cannot even be measured for the TFM image due to too high noise level, whereas the SDH can be rather satisfactorily detected by TFMp. The main point for this example is that the contrast of TFMp is more than 20 dB above that of TFM, for all reflectors.

978-1-5386-3383-0/17/$31.00 ©2017 IEEE

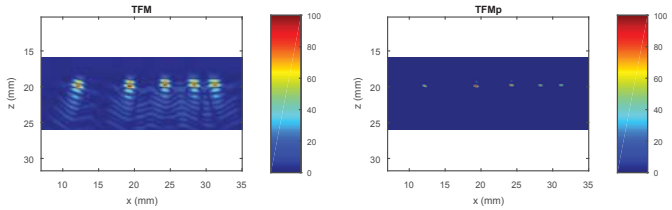

Fig. 4. Images obtained by TFM and TFMp for the second example. TFMp is tuned with $\mu = 70\ \%\ \mu_{max}$.

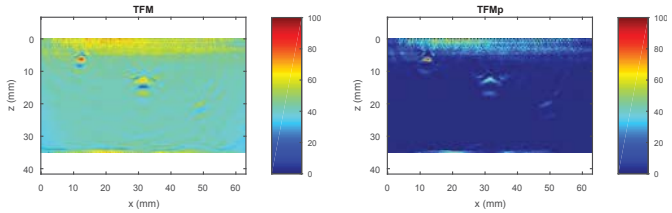

Fig. 5. Images obtained by TFM and TFMp for the third example. TFMp is tuned with $\mu = 50\ \%\ \mu_{max}$.

IV. Conclusion

In this paper we have proposed an improvement of the total focusing method (TFM) using an inverse problem approach. The signal model is obtained by formalizing the linear TFM imaging process. Therefore, no point spread function (PSF) is needed. The output data is then processed by minimizing an ℓ_1-norm-penalized least squares criterion. Three examples have been presented, and metrics for resolution and contrast measurements have been employed. TFMp gives much better lateral and axial resolution, and also a better contrast, than TFM. These two improvements indicate better flaw separation and detection abilities, respectively. When the specimen contains two close reflectors with respect to the inspection wavelength, the proposed approach allows good separation whereas TFM suffers from overlapping. In the presence of scattering noise, TFMp also achieves better detection capability.

The application of TFMp in real inspections is derived from its benefits. It can be used when close reflectors occur, for example when investigating flaws close to the backwall of a piece. It can also be an efficient denoising tool for imaging in noisy specimens. The next step of this work is therefore to apply this method to the detection and positioning of real flaws in realistic applications. It could be applied to a large variety of flaws such as lack of fusion, porosity, cracks, *etc.*

TABLE III
Metrics for the third example

	TFM		TFMp	
	Res. (mm)	***CNR (dB)***	***Res. (mm)***	***CNR (dB)***
Reflector #1	x: 2.90 z: 2.08	27.1	x: 2.29 z: 0.38	50.1
Reflector #2	x: 5.82 z: 2.95	23.9	x: 3.01 z: 1.05	46.5
Reflector #3	x: N/A z: N/A	18.8	x: 2.10 z: 0.63	40.8

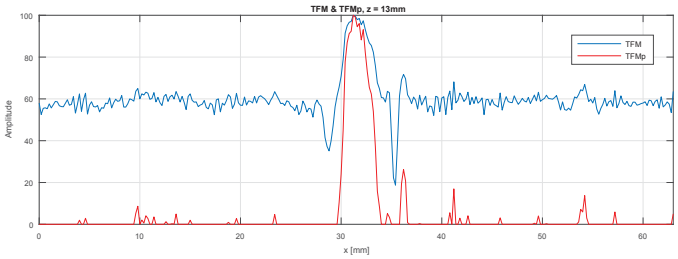

Fig. 6. Line for $z = 13$ mm for the third example.

References

[1] J. Seydel, "Ultrasonic synthetic-aperture focusing techniques in NDT," *Research techniques in nondestructive testing*, vol. 6, pp. 1–47, 1982.

[2] M. Karaman, P.-C. Li, and M. O'Donnell, "Synthetic aperture imaging for small scale systems," *IEEE Transactions on Ultrasonics, Ferroelectrics and Frequency Control*, vol. 42, no. 3, pp. 429–442, May 1995.

[3] C. Holmes, B. W. Drinkwater, and P. D. Wilcox, "Post-processing of the full matrix of ultrasonic transmit-receive array data for non-destructive evaluation," *NDT&E International*, vol. 38, no. 8, pp. 701–711, December 2005.

[4] J. Idier, *Bayesian Approach to Inverse Problems*. London, U.K.: ISTE Ltd and John Wiley & Sons Inc, April 2008.

[5] N. Quaegebeur and P. Masson, "Correlation-based imaging technique using ultrasonic transmit-receive array for non-destructive evaluation," *Ultrasonics*, vol. 52, no. 8, pp. 1056–1064, 2012.

[6] F. Lingvall, T. Olofsson, and T. Stepinski, "Synthetic aperture imaging using sources with finite aperture: Deconvolution of the spatial impulse response," *The Journal of the Acoustical Society of America*, vol. 114, no. 1, pp. 225–234, July 2003.

[7] G. A. Guarneri, D. R. Pipa, F. N. Junior, L. V. R. de Arruda, and M. V. W. Zibetti, "A sparse reconstruction algorithm for ultrasonic images in nondestructive testing," *Sensors*, vol. 15, no. 4, p. 9324, 2015.

[8] H. Wu, J. Chen, S. Wu, H. Jin, and K. Yang, "A model-based regularized inverse method for ultrasonic b-scan image reconstruction," *Measurement Science and Technology*, vol. 26, no. 10, p. 105401, 2015.

[9] C. Zala, "High-resolution inversion of ultrasonic traces," *IEEE Transactions on Ultrasonics, Ferroelectrics, and Frequency Control*, vol. 39, no. 4, pp. 458–463, July 1992.

[10] M. S. O'Brien, A. N. Sinclair, and S. M. Kramer, "Recovery of a sparse spike time series by ℓ_1 norm deconvolution," *IEEE Transactions on Signal Processing*, vol. 42, no. 12, pp. 3353–3365, December 1994.

[11] C. Soussen, J. Idier, E. Carcreff, L. Simon, and C. Potel, "Ultrasonic non destructive testing based on sparse deconvolution," *Journal of Physics: Conference Series*, vol. 353, p. 012018 (10 pages), 2012.

[12] E. Carcreff, S. Bourguignon, J. Idier, and L. Simon, "A linear model approach for ultrasonic inverse problems with attenuation and dispersion," *IEEE Transactions on Ultrasonics, Ferroelectrics and Frequency Control*, vol. 61, no. 7, pp. 1191–1203, July 2014.

[13] E. Carcreff, S. Bourguignon, A. Duclos, L. Simon, and J. Idier, "Detection of flat bottom holes using sparse deconvolution," *Physics Procedia*, vol. 70, pp. 558–561, 2015, proceedings of the 2015 ICU International Congress on Ultrasonics, Metz, France.

[14] J. Tropp and S. Wright, "Computational methods for sparse solution of linear inverse problems," *Proceedings of the IEEE*, vol. 98, no. 6, pp. 948–958, June 2010.

[15] G. Wahba, "Practical approximate solutions to linear operator equations when the data are noisy," *SIAM Journal on Numerical Analysis*, vol. 14, no. 4, pp. 651–667, 1977.

[16] G. H. Golub, M. Heath, and G. Wahba, "Generalized cross-validation as a method for choosing a good ridge parameter," *Technometrics*, vol. 21, pp. 215–223, May 1979.

[17] P. Stoica and Y. Selén, "Model-order selection: a review of information criterion rules," *IEEE Signal Processing Magazine*, vol. 21, no. 4, pp. 36–47, July 2004.

[18] M. Welvaert and Y. Rosseel, "On the definition of signal-to-noise ratio and contrast-to-noise ratio for fMRI data," *PLOS ONE*, vol. 8, no. 11, pp. 1–10, 11 2013.

978-1-5386-3383-0/17/$31.00 ©2017 IEEE